Bipolar Spherical Harmonics Expansions of the Boltzmann Transport Equation

K. Rupp[*,†], C. Jungemann[‡], M. Bina[†°], A. Jüngel[*], and T. Grasser[†]
[*]Institute for Analysis and Scientific Computing, TU Wien, Wiedner Hauptstraße 8-10/E101, A-1040 Wien, Austria
[†]Institute for Microelectronis, TU Wien, Gußhausstraße 27-29/E360, A-1040 Wien, Austria
[‡]Institut für Theoretische Elektrotechnik, RWTH Aachen, Kackertstraße 15-17, D-52072 Aachen, Germany
[°]Christian Doppler Laboratory for Reliability in Microelectronics at the Institute for Microelectronics, TU Wien, Austria
Email: {rupp|bina|grasser}@iue.tuwien.ac.at, Christoph.Jungemann@ithe.rwth-aachen.de, juengel@asc.tuwien.ac.at

***Abstract*—An extension of the spherical harmonics expansion method for the deterministic solution of the Boltzmann transport equation for the computation of both electron and hole distribution functions is presented. The generation and recombination of carriers via traps in the band gap is considered in a way that is consistent with the Shockley-Read-Hall model. Simulation results for a pn-diode and an n-MOSFET are presented, which are obtained with only a moderate increase in simulation time and memory requirements compared to unipolar simulations.**

I. Introduction

Since its introduction in the early 1990s [1], [2], the spherical harmonics expansion (SHE) method for the deterministic numerical solution of the Boltzmann transport equation (BTE) has evolved into an attractive alternative to the stochastic Monte Carlo (MC) method. Recent advances of the SHE method even allow for the accuracy of full-band MC at a fraction of the computational cost for three-dimensional device simulation [3], [4], further increasing the attractiveness of the method for modern TCAD. Moreover, the SHE method has already been applied successfully to problems where the MC method either fails to produce good results within a reasonable time budget, or fails completely [5].

The SHE method has so far been used for one carrier type only, while the other carrier type has been modeled by a continuity equation [6] or ignored at all [7]. However, due to the absence of generation and recombination in such a setting, secondary effects cannot be captured accurately. Furthermore, moment-based approaches are unable to describe the complex interaction of highly energetic carriers satisfactorily, since the distribution of charge carriers with respect to momentum cannot be fully recovered from macroscopic quantities such as carrier density or average carrier energy only. Consequently, a bipolar solution of the Boltzmann transport equation provides higher accuracy and versatility at reasonable computational cost.

II. Theory

A coupled system given by the Poisson equation and a BTE for each carrier type is considered in the following. More precisely, the system

$$-\epsilon\Delta\psi = \rho \ , \tag{1}$$

$$\frac{\partial f^{\mathrm{n}}}{\partial t} + L^{\mathrm{n}}\{f^{\mathrm{n}}\} = Q^{\mathrm{n}}\{f^{\mathrm{n}}, f^{\mathrm{p}}\} \tag{2}$$

$$\frac{\partial f^{\mathrm{p}}}{\partial t} + L^{\mathrm{p}}\{f^{\mathrm{p}}\} = Q^{\mathrm{p}}\{f^{\mathrm{n}}, f^{\mathrm{p}}\} \tag{3}$$

with permittivity ϵ, Laplace operator Δ, electrostatic potential ψ, space charge ρ, electron and hole distribution functions f^{n}, f^{p}, free-streaming operators L^{n}, L^{p}, and scattering operators Q^{n}, Q^{p} needs to be solved. To avoid notational clutter, only a single valley is considered, spin degeneracy is assumed, and the dependence on the spatial variable $\mathbf{x}$, the momentum $\hbar\mathbf{k}$ and time t is not written explicitly wherever appropriate. If $Q^{\mathrm{n}}\{f^{\mathrm{n}}, f^{\mathrm{p}}\} = Q^{\mathrm{n}}\{f^{\mathrm{n}}\}$ and $Q^{\mathrm{p}}\{f^{\mathrm{n}}, f^{\mathrm{p}}\} = Q^{\mathrm{p}}\{f^{\mathrm{p}}\}$, the two BTEs decouple, thus no generation or recombination events are considered. In this work we consider unipolar scattering processes Q^{n}_η and Q^{p}_η as well as generation and recombination processes via a single trap level in the band gap with occupation probability f^{t} [9]:

$$\begin{aligned} Q^{\mathrm{n}}\{f^{\mathrm{n}}, f^{\mathrm{p}}\} = \sum_\eta Q^{\mathrm{n}}_\eta\{f^{\mathrm{n}}\} + (1-f^{\mathrm{n}})\Gamma^{\mathrm{n}}_{\mathrm{G}} N^{\mathrm{t}} f^{\mathrm{t}} \\ - f^{\mathrm{n}}\Gamma^{\mathrm{n}}_{\mathrm{R}} N^{\mathrm{t}}(1-f^{\mathrm{t}}) \end{aligned} \tag{4}$$

with electron generation rate $\Gamma^{\mathrm{n}}_{\mathrm{G}}$ and electron recombination rate $\Gamma^{\mathrm{n}}_{\mathrm{R}}$, cf. Fig. 1. Here, the Pauli principle is considered in the conduction band and for the traps. Similarly, one obtains with hole generation rate $\Gamma^{\mathrm{p}}_{\mathrm{G}}$ and hole recombination rate $\Gamma^{\mathrm{p}}_{\mathrm{R}}$ the hole scattering operator

$$\begin{aligned} Q^{\mathrm{p}}\{f^{\mathrm{n}}, f^{\mathrm{p}}\} = \sum_\eta Q^{\mathrm{p}}_\eta\{f^{\mathrm{p}}\} + (1-f^{\mathrm{p}})\Gamma^{\mathrm{p}}_{\mathrm{G}} N^{\mathrm{t}}(1-f^{\mathrm{t}}) \\ - f^{\mathrm{p}}\Gamma^{\mathrm{p}}_{\mathrm{R}} N^{\mathrm{t}} f^{\mathrm{t}} \ . \end{aligned} \tag{5}$$

An extension to multiple trap levels without inter-trap interactions is obtained by a summation over all trap levels. However, we restrict our discussion to a single trap level for reasons of clarity.

Unipolar scattering processes for electrons and holes described by Q^{n}_η and Q^{p}_η such as phonon scattering or impurity scattering are treated in the usual manner [3]. Moreover, f^{n} and f^{p} are coupled via the trap occupancy f^{t}, for which the

K. Rupp, A. Jüngel, and T. Grasser acknowledge support by the Austrian Science Fund (FWF), grant P23598.

 ISBN 978-0-615-71756-2

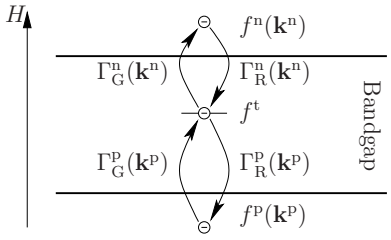

Fig. 1. Schematic for the generation and recombination of electrons (with rates $\Gamma^{\mathrm{n}}_{\mathrm{G}}$, $\Gamma^{\mathrm{n}}_{\mathrm{R}}$ and momentum $\hbar\mathbf{k}^{\mathrm{n}}$) and holes (with rates $\Gamma^{\mathrm{p}}_{\mathrm{G}}$, $\Gamma^{\mathrm{p}}_{\mathrm{R}}$ and momentum $\hbar\mathbf{k}^{\mathrm{p}}$) via a trap with occupation probability f^{t}. H denotes total energy.

rate equation is given by [9]

$$\frac{\partial f^{\mathrm{t}}}{\partial t} = \frac{1}{(2\pi)^3}\int_{\mathcal{B}} f^{\mathrm{n}}(\mathbf{k})\Gamma^{\mathrm{n}}_{\mathrm{R}}(\mathbf{k})(1-f^{\mathrm{t}}) - (1-f^{\mathrm{n}}(\mathbf{k}))\Gamma^{\mathrm{n}}_{\mathrm{G}}(\mathbf{k})f^{\mathrm{t}}\,\mathrm{d}\mathbf{k}^3\ , \tag{6}$$

where the integration is carried out over the Brillouin zone $\mathcal{B}$. In steady state, which is considered in the remainder of this work, the net generation/recombination rates of electrons and holes are equal, thus

$$\int_{\mathcal{B}} f^{\mathrm{n}}(\mathbf{k})\Gamma^{\mathrm{n}}_{\mathrm{R}}(\mathbf{k})(1-f^{\mathrm{t}}) - (1-f^{\mathrm{n}}(\mathbf{k}))\Gamma^{\mathrm{n}}_{\mathrm{G}}(\mathbf{k})f^{\mathrm{t}}\,\mathrm{d}\mathbf{k}^3 = \int_{\mathcal{B}} f^{\mathrm{p}}(\mathbf{k})\Gamma^{\mathrm{p}}_{\mathrm{R}}(\mathbf{k})f^{\mathrm{t}} - (1-f^{\mathrm{p}}(\mathbf{k}))\Gamma^{\mathrm{p}}_{\mathrm{G}}(\mathbf{k})(1-f^{\mathrm{t}})\,\mathrm{d}\mathbf{k}^3\ . \tag{7}$$

Since the trap occupancy f^{t} does not depend on the momentum $\hbar\mathbf{k}$, the explicit formula

$$f^{\mathrm{t}} = \Big[\int_{\mathcal{B}} \Gamma^{\mathrm{n}}_{\mathrm{R}}(\mathbf{k})f^{\mathrm{n}}(\mathbf{k})\,\mathrm{d}\mathbf{k}^3 + \int_{\mathcal{B}} \Gamma^{\mathrm{p}}_{\mathrm{G}}(\mathbf{k})(1-f^{\mathrm{p}}(\mathbf{k}))\,\mathrm{d}\mathbf{k}^3\Big] \Big/ \Big[\int_{\mathcal{B}} \Gamma^{\mathrm{n}}_{\mathrm{R}}(\mathbf{k})f^{\mathrm{n}}(\mathbf{k}) + \Gamma^{\mathrm{n}}_{\mathrm{G}}(\mathbf{k})(1-f^{\mathrm{n}}(\mathbf{k}))\,\mathrm{d}\mathbf{k}^3 + \int_{\mathcal{B}} \Gamma^{\mathrm{p}}_{\mathrm{R}}(\mathbf{k})f^{\mathrm{p}}(\mathbf{k}) + \Gamma^{\mathrm{p}}_{\mathrm{G}}(\mathbf{k})(1-f^{\mathrm{p}}(\mathbf{k}))\,\mathrm{d}\mathbf{k}^3\Big] \tag{8}$$

for the trap occupation probability is obtained, which implies $0 \leq f^{\mathrm{t}} \leq 1$ for $0 \leq f^{\mathrm{n}} \leq 1$ and $0 \leq f^{\mathrm{p}} \leq 1$. The recombination rates are

$$\Gamma^{\mathrm{n}}_{\mathrm{R}}(\mathbf{k}) = \sigma^{\mathrm{n}}v^{\mathrm{n}}(\mathbf{k})\ , \qquad \Gamma^{\mathrm{p}}_{\mathrm{R}}(\mathbf{k}) = \sigma^{\mathrm{p}}v^{\mathrm{p}}(\mathbf{k})\ , \tag{9}$$

while the generation rates at equilibrium are obtained by the principle of detailed balance [10] as

$$\Gamma^{\mathrm{n}}_{\mathrm{G}}(\mathbf{k}) = \sigma^{\mathrm{n}}v^{\mathrm{n}}(\mathbf{k})\exp\Big(\frac{H^{\mathrm{t}} - H^{\mathrm{n}}(\mathbf{k})}{k_{\mathrm{B}}T}\Big)\ , \tag{10}$$

$$\Gamma^{\mathrm{p}}_{\mathrm{G}}(\mathbf{k}) = \sigma^{\mathrm{p}}v^{\mathrm{p}}(\mathbf{k})\exp\Big(\frac{H^{\mathrm{p}}(\mathbf{k}) - H^{\mathrm{t}}}{k_{\mathrm{B}}T}\Big)\ , \tag{11}$$

with trap capture cross sections σ^{n} and σ^{p}, velocities v^{n} and v^{p}, total trap energy H^{t}, and total carrier energies $H^{\mathrm{n}}(\mathbf{k})$, $H^{\mathrm{p}}(\mathbf{k})$ in the conduction and the valence bands, respectively. It is important to note that (4)-(11) are the fundamental equations used in the derivation of the Shockley-Read-Hall (SRH) model before further approximations are applied in order to obtain closed-form solutions [11].

III. Spherical Harmonics Expansions

The spherical harmonics expansion needs to be applied to the system (1)-(5) with (6) in the transient case or (8) in steady state. Since only the scattering operators are modified with respect to two separate unipolar solutions of the BTEs, it is sufficient to consider the projections of (4) and (5). Additionally, f^{n} does not occur explicitly in the BTE for f^{p} and vice versa. Thus, f^{n} and f^{p} are only implicitly coupled via the trap occupancy f^{t}, which does not depend on the wave vector and hence does not interfere with projections in momentum space. Multiplication of a spherical harmonic $Y_{l,m}$, multiplication with a delta distribution for integration over equi-energy surfaces, and integration over the Brillouin zone results in

$$Q^{\mathrm{n}}_{l,m}\{f^{\mathrm{n}}, f^{\mathrm{p}}\} = \sum_{\eta} Q^{\mathrm{n}}_{\eta;l,m}\{f^{\mathrm{n}}\} + \Big(\frac{\delta_{0,0;l,m}}{Y_{0,0}} - f^{\mathrm{n}}_{l,m}\Big)\Gamma^{\mathrm{n}}_{\mathrm{G}}N^{\mathrm{t}}f^{\mathrm{t}}Z^{\mathrm{n}} - f^{\mathrm{n}}_{l,m}\Gamma^{\mathrm{n}}_{\mathrm{R}}N^{\mathrm{t}}(1-f^{\mathrm{t}})Z^{\mathrm{n}} \tag{12}$$

for electrons, and

$$Q^{\mathrm{p}}_{l,m}\{f^{\mathrm{n}}, f^{\mathrm{p}}\} = \sum_{\eta} Q^{\mathrm{p}}_{\eta;l,m}\{f^{\mathrm{p}}\} + \Big(\frac{\delta_{0,0;l,m}}{Y_{0,0}} - f^{\mathrm{p}}_{l,m}\Big)\Gamma^{\mathrm{p}}_{\mathrm{G}}N^{\mathrm{t}}(1-f^{\mathrm{t}})Z^{\mathrm{p}} - f^{\mathrm{p}}_{l,m}\Gamma^{\mathrm{p}}_{\mathrm{R}}N^{\mathrm{t}}f^{\mathrm{t}}Z^{\mathrm{p}}\ . \tag{13}$$

for holes. Here, the orthonormality of spherical harmonics on the unit sphere has been used, $Q^{\mathrm{n}}_{\eta;l,m}$ and $Q^{\mathrm{p}}_{\eta;l,m}$ denote the projected unipolar scattering operators, Z^{n} and Z^{p} are the isotropic approximations to the densities of states in the conduction and the valence band, respectively [3], [8], and $\delta_{0,0;l,m}$ is zero unless $l = m = 0$, in which case it is one. Note that if the Pauli principle is ignored in the conduction and in the valence bands, which is commonly the case in order to obtain linear scattering operators for a majority of scattering processes, only the regeneration terms containing $\Gamma^{\mathrm{n}}_{\mathrm{R}}$ and $\Gamma^{\mathrm{p}}_{\mathrm{R}}$ depend on the expansion coefficients $f^{\mathrm{n}}_{l,m}$ and $f^{\mathrm{p}}_{l,m}$. On the other hand, the Pauli principle must not be ignored for the traps in order to model the underlying physical processes correctly.

IV. Results

The proposed bipolar SHE method is implemented in our free, multi-dimensional open-source SHE simulator ViennaSHE [13], which is used for all simulations considered in the following. Devices at room temperature are simulated using capture cross sections $\sigma^{\mathrm{n}} = \sigma^{\mathrm{p}} = 3.2 \times 10^{-16}$ cm^2 [9]. Timings are taken on a machine equipped with a AMD II X2 255 dual-core processor.

First, the self-consistent one-dimensional simulation of a 500 nm pn-diode with a doping of 10^{16} cm^{-3} in the n- and p-region, respectively, and 400 spatial grid points is considered. An energy spacing of 12.5 meV is used, while the energy range is chosen such that the kinetic energy range in

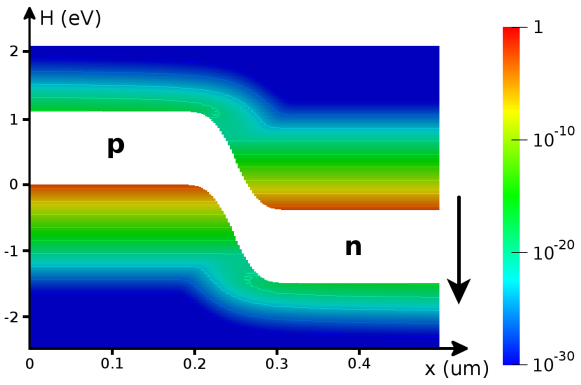

Fig. 2. Electron (top) and hole (bottom) energy distribution functions of a pn-diode in reverse bias.

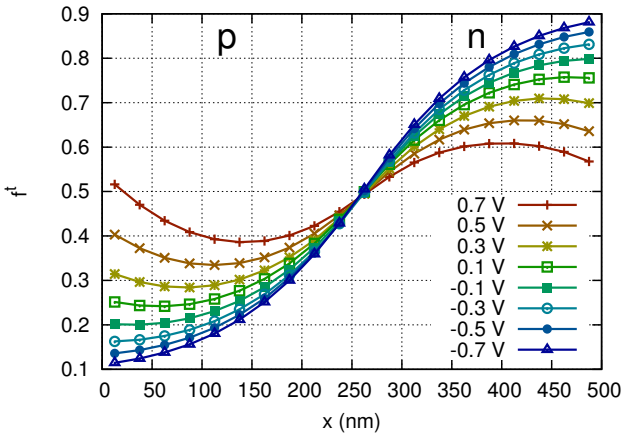

Fig. 3. Trap occupancy f^{t} in the pn-diode.

both the conduction and the valence band extends to at least 1 eV. The trap density is taken to be 10^{15} cm^{-3} uniformly over the device. Acoustic and optical phonon scattering as well as ionized impurity scattering are included as linear scattering operators. The energy distribution functions (EDFs) for both carrier types of the simulated reverse-biased pn-diode is depicted in Fig. 2, where the conduction and valence band edge as well as the band gap is readily visible. An energy barrier due to the reverse bias for electrons willing to travel from the n-region to the p-region and vice versa for holes is also visible in the distribution function.

The trap occupancy f^{t} for a trap-level 0.1 eV above the center of the band gap along the diode is shown in Fig. 3. At reverse bias, traps are increasingly occupied in the n-region, while the p-region is depleted. With increasing forward bias, the trap occupancy becomes almost uniform over the device.

The comparison of the number of even-order SHE unknowns entering the linear solver for various bias conditions in Fig. 4 shows an overall increase by a factor of two compared to unipolar SHE for each nonlinear iteration step for the solution of the coupled Boltzmann-Poisson system. The linear

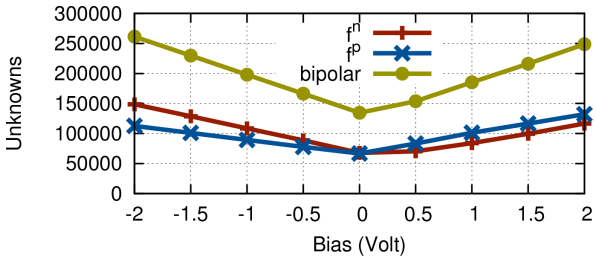

Fig. 4. Comparison of the even-order unknowns for unipolar and bipolar SHE. The number of unknowns depends almost linearly on the applied bias due to the H-transform.

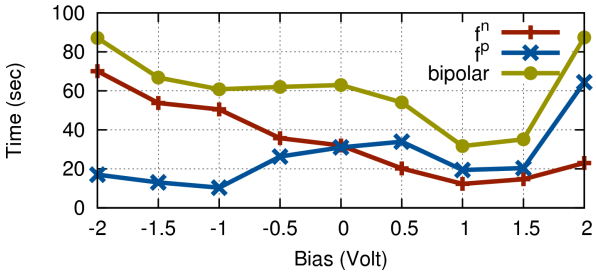

Fig. 5. Comparison of linear solver time per nonlinear iteration for unipolar and bipolar SHE. A fluctuation by more than a factor of two is observed in the bipolar case.

dependence of the number of unknowns on the applied bias is a consequence of the H-transform [14].

Fig. 5 illustrates the single-threaded linear solver execution times obtained in each nonlinear Gummel iteration step. Depending on the polarity of the applied bias, the total solution time is dominated by one of the two carrier types. Furthermore, an increase of the solver time at higher bias is observed, which is, however, also visible in the unipolar case.

The EDFs obtained from the simulation of an n-MOSFET with a channel length of 100 nm, the same trap parameters as for the pn-diode, and at two different bias conditions using bipolar SHE on an unstructured, spatially triangular grid are depicted in Fig. 6. For simplicity, the EDFs are clamped to an equilibrium Maxwell distribution at the source and drain contacts, which leads to a boundary layer in the solution at the contacts. This allows for a direct comparison of the EDFs for heated electrons in the drain region as well as heated holes in the source region with the equilibrium Maxwell distributions. For the case of a high gate voltage, a resistor-like linear shape of the conduction band edge from the source towards the drain is obtained. However, at low gate voltage, where the device is in saturation mode, a high voltage drop between channel and drain region is obtained. The electron distribution function indicates a smaller electron population at the end of the channel than for a high gate voltage.

Fig. 7 illustrates the computed trap occupancies f^{t} in the n-MOSFET at two different operating conditions. At high gate bias, trap occupancies right below the gate oxide are increased, which stems from the formation of the channel. A low occupancy is obtained in the source region, while a high occupancy

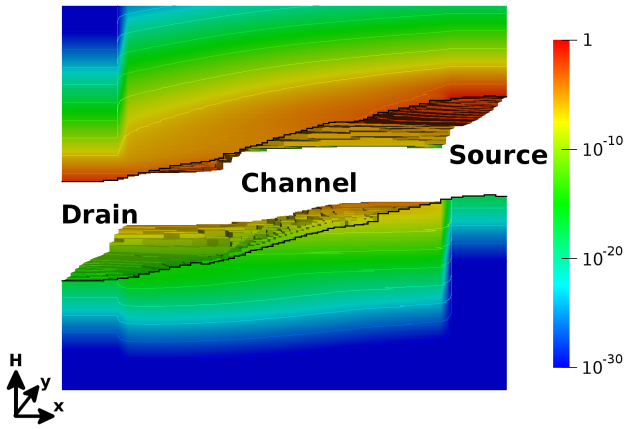

(a) $V_{\mathrm{DS}} = 1$ Volt, $V_{\mathrm{G}} = 1.2$ Volt.

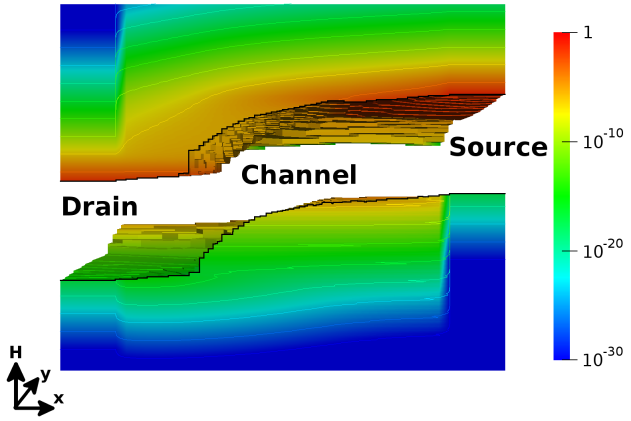

(b) $V_{\mathrm{DS}} = 1$ Volt, $V_{\mathrm{G}} = 0.2$ Volt.

Fig. 6. Energy distribution functions in an n-MOSFET at two different operating conditions.

is obtained in the drain region. Conversely, for the case of low applied gate voltage, only a very low trap occupancy is obtained right below the gate oxide. Nevertheless, the high occupancy in the drain region is similar to the case of a high gate voltage.

V. Conclusion

The first self-consistent device simulations using the SHE method for deterministic numerical solutions of the Boltzmann-Poisson system for both carrier types are presented. The doubling of the number of unknowns and the moderate increase in simulation times compared to unipolar SHE are a small price to pay for the many new possibilities such as the modeling of high energy effects. For example, a bipolar SHE method paves the way for studies of avalanche effects due to impact ionization at a much higher amount of detail than with macroscopic models, while simulation times are orders of magnitude smaller than with the MC method.

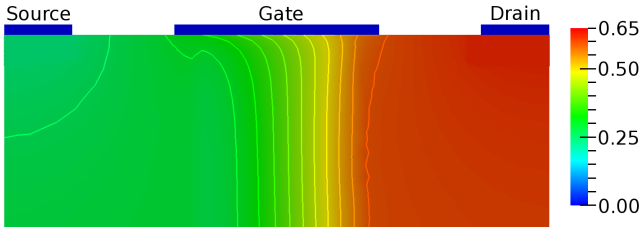

(a) $V_{\mathrm{DS}} = 1$ Volt, $V_{\mathrm{G}} = 1.2$ Volt.

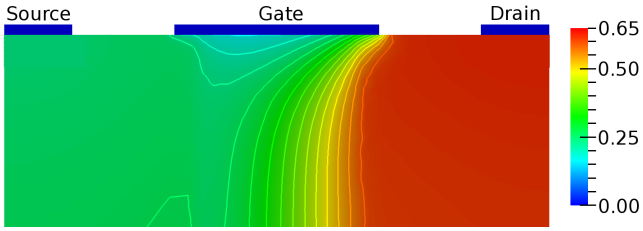

(b) $V_{\mathrm{DS}} = 1$ Volt, $V_{\mathrm{G}} = 0.2$ Volt.

Fig. 7. Trap occupancy in the simulated MOSFET device at two different operating conditions with a contour spacing of 0.033.

References

[1] N. Goldsman, L. Henrickson, and J. Frey, "A physics-based analytical/numerical solution to the Boltzmann transport equation for the use in device simulation", *Solid-State Electronics*, vol. 34, pp. 389–396, 1991.

[2] A. Gnudi, D. Ventura, and G. Baccarani, "One-dimensional simulation of a bipolar transistor by means of spherical harmonics expansion of the Boltzmann transport equation", *Proc. SISDEP*, vol. 4, pp. 205–213, 1991.

[3] S.-M. Hong, A.-T. Pham, and C. Jungemann, *Deterministic solvers for the Boltzmann transport equation*, Springer, 2011.

[4] K. Rupp, T. Grasser and A. Jüngel, "On the feasibility of spherical harmonics expansions of the Boltzmann transport equation for three-dimensional device geometries", *IEDM Techn. Digest*, 2011.

[5] B. Meinerzhagen, A. T. Pham, S.-M. Hong, and C. Jungemann, "Solving Boltzmann transport equation without Monte-Carlo algorithms – new methods for industrial TCAD applications", *Proc. SISPAD*, pp. 293-296, 2010.

[6] H. Lin, N. Goldsman, and I. D. Mayergoyz, "Deterministic BJT modeling by self- consistent solution to the Boltzmann, Poisson and hole-continuity equations", *Proc. IWCE*, pp. 55–59, 1993.

[7] K. Rahmat, J. White, and D. A. Antoniadis, "Simulation of semiconductor devices using a Galerkin/spherical harmonic expansion approach to solving the coupled Poisson-Boltzmann system", *IEEE Transactions on Computer-Aided Design of Integrated Circuits and Systems*, vol. 15, no. 10, pp. 1181–1195, 1996.

[8] S. Jin, S.-M. Hong, and C. Jungemann, "An efficient approach to include full-band effects in deterministic Boltzmann equation solver based on high-order spherical harmonics expansion", *IEEE Transactions on Electron Devices*, vol. 58, no. 5, pp. 1287–1294, 2011.

[9] C. Jungemann, "A deterministic solver for the Langevin Boltzmann equation including the Pauli principle", *Noise and Fluctuations in Circuits, Devices, and Materials*, vol. 6600, no. 1, pp. 660007, 2007.

[10] O. Madelung, *Introduction to solid state theory*, Springer, 1978.

[11] W. Shockley and W. T. Read, "Statistics of the recombinations of holes and electrons", *Physical Review*, vol. 87, no. 5, pp. 835-842, 1952.

[12] K. Rupp, P. W. Lagger, T. Grasser, and A. Jüngel, "Inclusion of carrier-carrier-scattering into arbitrary-order spherical harmonics expansions of the Boltzmann transport equation", *Proc. IWCE*, 2012.

[13] ViennaSHE. http://viennashe.sourceforge.net/

[14] A. Gnudi, D. Ventura, G. Baccarani, and F. Odeh, "Two-dimensional MOSFET simulation by means of a multidimensional spherical harmonics expansion of the Boltzmann transport equation." *Solid-State Electronics*, vol. 36, no. 4, pp. 575–581, 1993.